ORIGINAL PAPER

An Integrated Index for the Identification of Diabetic Retinopathy Stages Using Texture Parameters

U. Rajendra Acharya · E. Y. K. Ng · Jen-Hong Tan ·
S. Vinitha Sree · Kwan-Hoong Ng

Abstract Diabetes is a condition of increase in the blood sugar level higher than the normal range. Prolonged diabetes damages the small blood vessels in the retina resulting in diabetic retinopathy (DR). DR progresses with time without any noticeable symptoms until the damage has occurred. Hence, it is very beneficial to have the regular cost effective eye screening for the diabetes subjects. This paper documents a system that can be used for automatic mass screenings of diabetic retinopathy. Four classes are identified: *normal retina*, *non-proliferative diabetic retinopathy (NPDR)*, *proliferative diabetic retinopathy (PDR)*, and *macular edema (ME)*. We used 238 retinal fundus images in our analysis. Five different texture features such as homogeneity, correlation, short run emphasis, long run emphasis, and run percentage were extracted from the digital fundus images. These features were fed into a support vector machine classifier (SVM) for automatic classification. SVM classifier of different kernel functions (linear, radial basis function, polynomial of order 1, 2, and 3) was studied. Receiver operation characteristics (ROC) curves were plotted to select the best classifier. Our proposed system is able to identify the unknown class with an accuracy of 85.2%, and sensitivity, specificity, and area under curve (AUC) of 98.9%, 89.5%, and 0.972 respectively using SVM classifier with polynomial kernel of order 3. We have also proposed a new integrated DR index (IDRI) using different features, which is able to identify the different classes with 100% accuracy.

Keywords Diabetes · Retinopathy · Classifier · Texture · Support vector machine · Fundus image · Index

Introduction

Diabetic retinopathy is a major cause of visual impairment all over the world [13]. More specifically, it represents an end-organ response to a systemic disease and it is a significant risk factor for vision loss and blindness. Individuals with diabetes are 25 times more likely to become blind as compared to the general population [25]. Hence, detecting the DR at the early stage will prevent the loss of vision.

Figure 1 shows the anatomy of the human eye. The retina is a thin layer of tissue that covers the inner part of the eye. The tissue is made of chemical photo detector cells. These detector cells are of two main types: the rods and the cones. Rods function in dim light and provide black-and-white vision, and the cones support daytime vision and color perception. These detector cells are not equally dense within the area of the retina. This is considered as sampling with an unequal (spatial) sampling interval. The result of the detection process is an electrical signal which is sent to the brain via the optic nerve. The optic disk is an area of the eye where the optic nerves leave the eye, leading to the brain, and therefore there is no detector cells in this area.

U. R. Acharya (✉)
Department of Electronics and Computer Engineering,
Ngee Ann Polytechnic,
Singapore, Singapore
e-mail: aru@np.edu.sg

E. Y. K. Ng · J.-H. Tan · S. V. Sree
School of Mechanical and Aerospace Engineering,
College of Engineering, Nanyang Technological University,
50, Nanyang Avenue,
Singapore 639798, Singapore

K.-H. Ng
Department of Biomedical Imaging, University of Malaya,
Kuala Lumpur, Malaysia
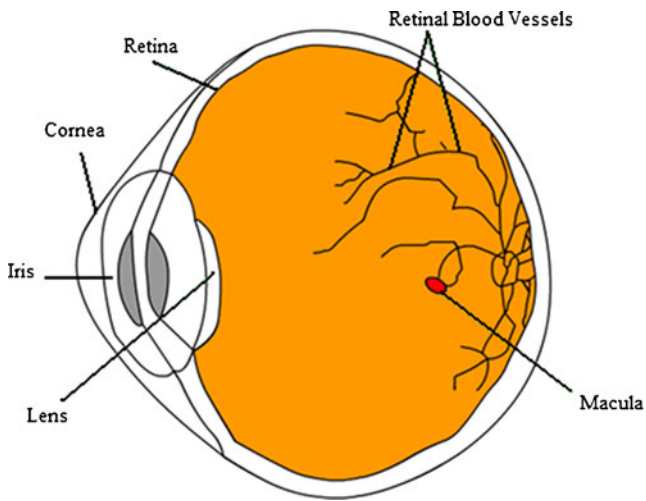
Fig. 1 Anatomy of human eye

This causes a break in the visual field, which is known as the "blind spot". The macula is an oval spot located in the center of the retina and is responsible for the acuteness of vision. The fovea is located in the center of the macula. It helps in discriminating colors and has the highest density of photo detector cells.

The earliest disease related changes can be seen in the retina. A brief description of the different stages of DR is given below and also tabulated in Table 1 [21]. Table 2 presents the risk of macular edema associated with the various symptoms.

- **Mild non-proliferative diabetic retinopathy (Mild NPDR) (grade 1)**: has the presence of at least one microaneurysm with or without hard exudates, cotton wool spots or haemorrhages.
- **Moderate non-proliferative diabetic retinopathy (Moderate NPDR) (grade 2)**: is characterized by the presence of more microaneurysms and retinal haemorrhages. Cotton wool spots and a limited amount of venous beading may also be present.

Table 1 Information about retinopathy grade provided by medical experts

Retinopathy grade	Definition
Grade 0 (Normal)	$(\mu A=0)$ and $(H=0)$
Grade 1	$(0 < \mu A \leq 5)$ and $(H=0)$
Grade 2	$((5 < \mu A < 15)$ or $(0 < H < 5))$ and $(NV=0)$
Grade 3	$(\mu A \geq 15)$ or $(H \geq 5)$ OR $(NV=1)$

Where μA represents the number of microaneurysms, H represents the number of hemorrhages, NV represents the presence (1) or absence (0) of neovascularization

Table 2 Information about the risk of Macular Edema (provided by medical experts)

Risk of Macular Edema	Definition
0	No visible hard exudates
1	Shortest distance between macula and hard exudates
	> one papilla diameter
2	Shortest distance between macula and hard exudates
	≤ one papilla diameter

- **Severe non-proliferative diabetic retinopathy (Severe NPDR) (grade 2)**: More microaneurysms, retinal haemorrhages and hard exudates appear in this stage.
- **Proliferative diabetic retinopathy (PDR) (grade 3)**: is the advanced stage; the signals sent by the retina for nourishment pave way for the growth of new blood vessels. These new blood vessels are thin and fragile. It may result in severe loss of vision and even blindness, if they leak blood.
- **Macular edema (ME)**: In this case, there are fluid and protein deposits on or near the macula causing it to thicken and swell. This swelling may distort the vision, as the macula is near the retina at the back of the eyeball.

Diabetic retinopathy is one of the most common causes of visual impairment among working class people in developed countries [6]. The digital fundus images of diabetes subjects can be examined once in every year to avoid the progression of disease and to ensure timely treatment [2]. The use of laser photocoagulation may slow down the progression of DR. To aid in easier DR screening process, recently, there has been an increase in the application of digital image processing and data mining techniques for the automatic detection of DR stages [23]. Some of the studies using image processing techniques for abnormality detection in the fundus images are described in this section. Literature pertaining to the use of classifiers for DR stage detection is presented in the Discussion section of the paper.

A computer aided diagnosis system to assist physicians to detect abnormalities associated with fundus images of the retina was developed [9]. Based on a study using 450 fundus images, this system was found to identify blood vessel intersections and also detect the abnormal widths in blood vessels. A three-step approach for the detection and classification of bright lesions fundus images was presented [29]. The steps involve local contrast enhancement (pre-processing stage), use of improved fuzzy C-Means (IFCM) to segment bright lesion areas, and the use of hierarchical

support vector machine (SVM) for classification. Their approach successfully classified bright non-lesion areas, exudates, and cotton wool spots.

A neural network was used to detect diabetic features namely vessels, exudates, and haemorrhages in fundus images, and the performance of the network was compared against an ophthalmologist screening [5]. Detection rates for the recognition of vessels, exudates, and haemorrhages were 91.7%, 93.1%, and 73.8% respectively. The system can be used as an aid for screening of diabetic patients for retinopathy disease. A novel red lesion detection method was presented based on a hybrid approach [16]. They were able to detect the red lesions with a sensitivity of 100% at a specificity of 87%. The method was compared with several different automatic systems and was shown to perform better than them. Moreover, its performance was close to that of a human expert examining the images for the presence of red lesions.

A new method to measure the severity of retinal arteriolar narrowing by calculating the arteriolar-to-venular diameter ratio (AVR) was proposed [7]. The blood vessels were detected using a combined Kalman filter and Gaussian filter. Their results indicate a 97.1% success rate in the identification of vessel starting points, and a 99.2% success rate in the tracking of retinal vessels.

Diabetic retinopathy may advance from mild to severe NPDR. A novel method for the automated detection and classification of vascular abnormalities in diabetic retino pathy was presented [3]. The vascular abnormalities were detected using scale and orientation selective Gabor filter banks. The proposed method classifies the fundus images into mild or severe stages using these Gabor filters.

In all the above discussed work, authors have automatically detected the DR stages using different features namely blood vessels, exudates, microaneurysms or haemorrhages etc. with higher accuracy. In this work, we extracted five features using texture image processing techniques and fed them to the SVM classifier for automatic identification of normal and diabetic retinopathy classes. The proposed scheme of the work is shown in Fig. 2. The layout of the paper is as follows: "Data Acquisition" presents the data acquisition process, and "Preprocessing" deals with the preprocessing of the raw images. "Texture Analysis" explains the extraction of the features using image processing techniques, and "Classifier Used" of the paper discusses the SVM classifier used. "Results" presents the results obtained, and the discussion on our data analysis is presented in "Discussion". Finally, the paper concludes in "Conclusion".

Data acquisition

In this work, the images used were extracted from MESSI-DOR database (http://messidor.crihan.fr). It has been esta
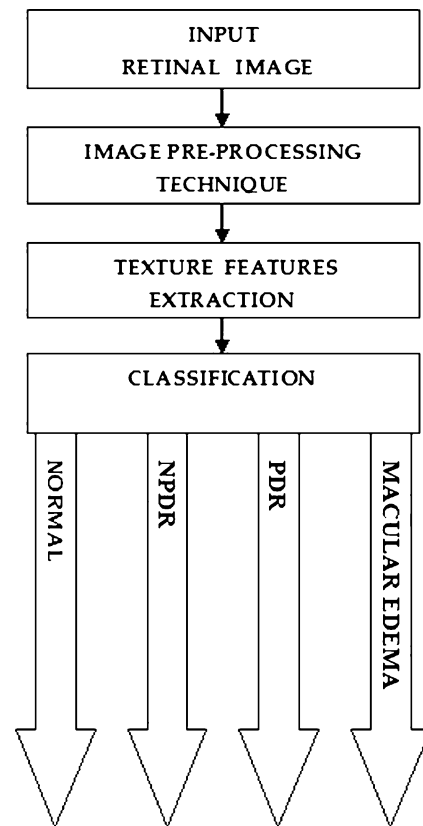
Fig. 2 Proposed system for the detection of the various diabetic retinopathy stages

blished to felicitate the computer aided diagnosis of DR. 1,200 eye fundus color images of the posterior pole for the database were acquired by 3 ophthalmologic departments using a color video 3CCD camera on a Topcon TRC NW6 non-mydriatic retinograph with a 45°FOV and were stored in sizes of either 1,440*960, or 2,240*1,488, or 2,304*1,536 pixels with 8 bits per color plane. 800 images were acquired with pupil dilation (one drop of Tropicamide at 0.5%) and 400 without dilation (http://messidor.crihan.fr). The details of the grades of the studied fundus DR images along with the risk of ME (according to medical experts) are shown in Table 3. In this work, we have used 180 fundus images belonging to the five classes, normal, mild NPDR, moderate NPDR, severe and ME and its details are shown in Table 3 (Fig. 3).

Preprocessing

Preprocessing was performed to remove the non-uniform background which may be due to non-uniform illumination or variation in the pigment color of eye. Adaptive histogram equalization operation was performed to solve this problem [20]. This technique computes several histograms, each

Table 3 Number of retinal images: (a) in each grade (b) in each DR class

Class	Number of images
(a)	
Grade 0	60
Grade 1-0	16
Grade 2-0	24
Grade 3-0	33
Grade 3-1	17
Grade 3-2	15
Grade 3-3	15
(b)	
Normal	60
NPDR	40
PDR	50
ME	30

(The first letter denotes grade and second letter indicates risk of ME)

corresponding to a distinct section of the image, and uses them to redistribute the lightness values of the image. Subsequently, these images were converted to grayscale.

Texture analysis

In this study, two groups of texture features were extracted from each retinal image: features derived from gray level co-occurrence matrix (GLCM) and run-length matrix [10, 19, 22, 24, 28].

Co-occurrence matrix

For an image of size M × N, the gray level co-occurrence matrix (GLCM) is defined as [10]

$$C_d(i,j) = |\{(p,q),(p+\Delta x, q+\Delta y): I(p,q)=i, I(p+\Delta x, q+\Delta y)=j\}| \tag{1}$$

Where $(p,q), (p+\Delta x, q+\Delta y) \in M \times N$, $d = (\Delta x, \Delta y)$ and $|\cdot|$ denotes the cardinality of a set. Given a grey level i in an image, the probability that the gray level of a pixel at a $(\Delta x, \Delta y)$ distance away is j is

$$P_d(i,j) = \frac{C_d(i,j)}{\sum C_d(i,j)} \tag{2}$$

From each co-occurrence matrix we computed the following features:

$$\text{Contrast}: \sum_i \sum_j (i-j)^2 P_d(i,j) \tag{3}$$

Contrast is the measurement of the local variations or differences in the GLCM. It works by measuring how elements do not lie on the main diagonal and returns a measure of the intensity contrast between a pixel and the neighboring pixels over the whole image. Large contrast reflects large intensity difference in GLCM.

$$\text{Homogeneity}: \sum_i \sum_j \frac{1}{1+(i-j)^2} P_d(i,j) \tag{4}$$

Homogeneity measures how close the distribution of elements in the GLCM is to the diagonal of GLCM. Homogeneity weighs values by the inverse of the contrast weight, with weights decreasing exponentially away from the diagonal as shown in Eq. 4 [19]. The addition of value '1' in the denominator is to prevent the value '0' during division. As homogeneity increases, the contrast typically decreases.
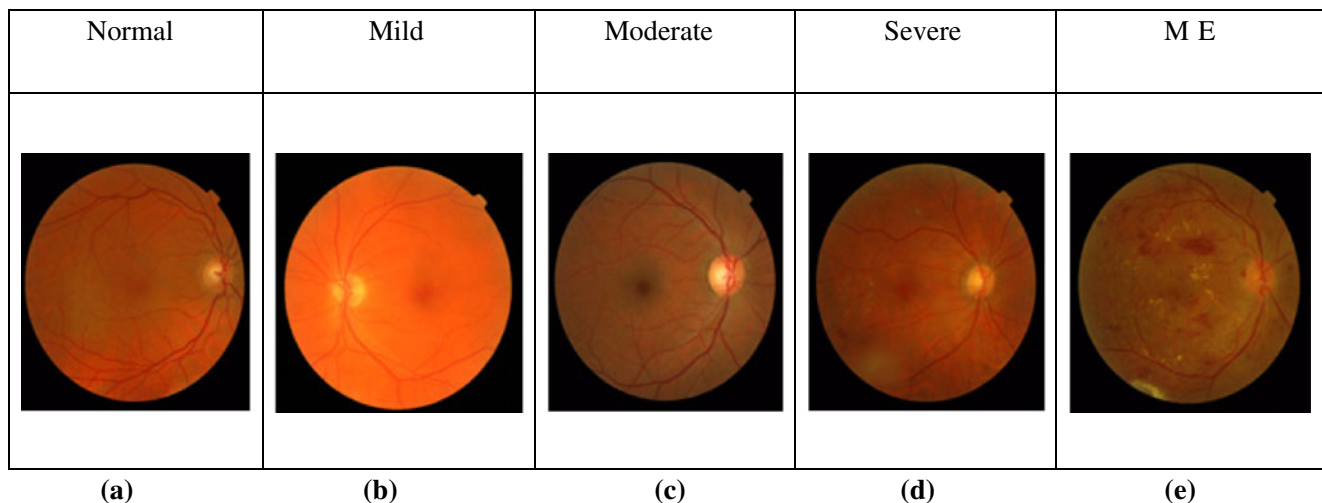
Fig. 3 Typical fundus images: **a** normal, **b** mild NPDR, **c** moderate NPDR, **d** severe NPDR, **e** ME

$$\text{Entropy} : En = -\sum_i \sum_j P_d(i,j) \cdot \ln P_d(i,j) \qquad (5)$$

Entropy is understood from the concept of thermodynamics. It is the randomness or the degree of disorder present in the image. The value of entropy is the largest when all elements of the co-occurrence matrix are the same and small when elements are unequal.

$$\text{Energy} = \sqrt{\text{Angular Second Moment}} \qquad (6)$$

and

$$\text{Angular Second Moment} : \sum_i \sum_j P_d^2(i,j) \qquad (7)$$

Energy is sometimes derived from the use of angular second moment [19]. It is the sum of squared elements in the GLCM known as angular second moment. Basically, it is the measurement of the denseness or order in the image. Moments 1–4 are defined as:

$$m_g = \sum_i \sum_j (i-j)^g P_d(i,j) \qquad (8)$$

where g is the integer power exponent that defines the moment order. Moments are the statistical expectation of certain power functions of a random variable and are characterized as follows [22]: moment 1 is the mean which is the average of pixel values in an image [24]; moment 2 is the standard deviation; moment 3 measures the degree of asymmetry in the distribution; and moment 4 measures the relative peakedness or flatness of a distribution and is also known as kurtosis [28].

Difference Statistics are defined as the distribution of probability $P_\delta(k)$ ($k = 0, \ldots, n-1$), and k is gray level difference between the points separated by δ in an image [17]. They are a subset of co-occurrence matrix and the distribution of probability $P_\delta(k)$ is defined as:

$$P_\delta(k) = \sum_i \sum_j C_d(i,j) \qquad (9)$$

Four such features are computed as follows [12].

$$\text{Angular second moment(ASM)} : \sum_{k=0}^{n-1} P_\delta(k)^2 \qquad (10)$$

When the $P_\delta(k)$ values are very similar or close, ASM is small. ASM is large when certain values are high and others are low.

$$\text{Contrast} : \sum_{k=0}^{n-1} k^2 P_\delta(k) \qquad (11)$$

Contrast is also known as the second moment of P_δ (its moment of inertia about the origin).

$$\text{Mean} : \sum_{k=0}^{n-1} k P_\delta(k) \qquad (12)$$

When $P_\delta(k)$ values are concentrated near the origin, mean is small and mean is large when they are far from the origin.

$$\text{Entropy} : -\sum_{k=0}^{n-1} P_\delta(k) \log P_\delta(k) \qquad (13)$$

Entropy is smallest when $P_\delta(k)$ values are unequal, and largest when $P_\delta(k)$ values are equal. Entropy is directly proportional to unpredictability.

The above mentioned features were calculated for $\delta = (0, 1)$, (1, 1), (1, 0), and the total mean values on the four features were taken.

Run length matrix

Run length method allows extraction of higher order statistical texture features. Run length matrix, P_θ (i,j), records the frequency that j points with a gray level i continue in the direction θ. The (i)[th] dimension of the matrix corresponds to the gray level and has a length equal to the maximum gray level, n, while (j)[th] corresponds to the run length and has length equal to the maximum run length, l. Five measures from run-length matrixes of $\theta = 0°$, 45°, 90°, and 135° were computed by as follows [15].

Table 4 Range of textural features extracted from the DR images

Features	Normal	Moderate	Severe	ME	P value
Homogeneity	0.63888±2.011E-02	0.65361±1.978E-02	0.57862±1.830E-02	0.62436±1.317E-02	<0.0001
Correlation	0.99824±2.088E-04	0.99824±3.152E-04	0.99799±3.217E-04	0.99814±2.255E-04	<0.0001
ShortRunEmphasis	0.78200±2.050E-02	0.77715±1.789E-02	0.81651±1.320E-02	0.79262±1.179E-02	<0.0001
LongRunEmphasis	3.4911±0.109	3.9487±9.973E-02	2.4114±9.626E-02	3.1962±9.734E-02	<0.0001
RunPer	2.5553±6.505E-02	2.4904±6.607E-02	2.7958±5.025E-02	2.6103±3.981E-02	<0.0001

Short run emphasis : $\displaystyle\sum_i \sum_j \frac{P_\theta(i,j)}{j^2} / \sum_i \sum_j P_\theta(i,j)$

(14)

Short run lengths are emphasized by dividing each run length value by the square of its length. The total number of runs in the image is the denominator [4].

Long run emphasis : $\displaystyle\sum_i \sum_j j^2 P_\theta(i,j) / \sum_i \sum_j P_\theta(i,j)$ (15)

In order to allow higher weight to the long runs, each run length value is multiplied by the square of its length [4].

Run Percentage : $\displaystyle\sum_i \sum_j P_\theta(i,j)/A$ (16)

A is the area of the image. This particular feature is the ratio between the total number of observed runs in image and the total number of possible runs if all runs had a length of one [4].

Gray Level Non − uniformity : $\displaystyle\sum_i \left\{ \sum_j P_\theta(i,j) \right\}^2 / \sum_i \sum_j P_\theta(i,j)$

(17)

This feature depends on high run length values. The gray level non-uniformity feature will have its lowest value if the runs are evenly distributed over all gray levels [4].

Run Length Non − uniformity : $\displaystyle\sum_j \left\{ \sum_i P_\theta(i,j) \right\}^2 / \sum_i \sum_j P_\theta(i,j)$

(18)

This feature will be the lowest if the runs are evenly distributed over all runs lengths [4].

Classifier used

In this work, we tested the support vector machine classifier with various kernel functions such as linear, radial basis function (RBF), polynomial function of order 1, order 2 and order 3 for classification. A brief description of the classifier and these kernel functions is given below.

SVM is one of the leading methods for solving non-linear classification problems. An SVM classifier uses supervised learning method that produces input-output mapping functions from a set of labeled training data. The mapping function can be either a regression function or a classification function. The objective of SVM modeling is
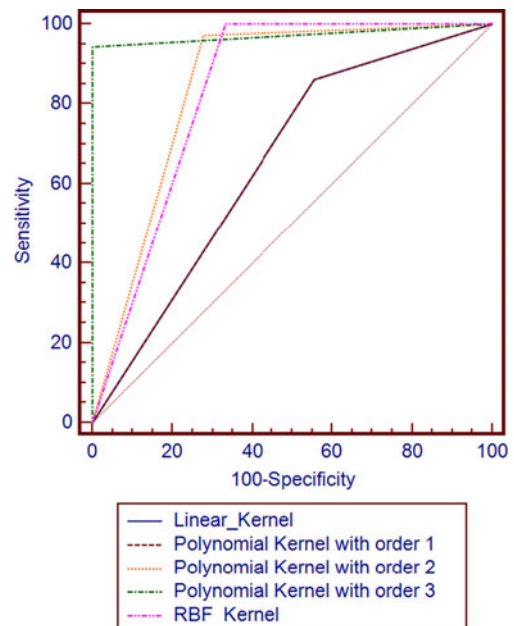
Fig. 4 ROC for various classifiers

to find a separating hyper-plane which separates positive and negative examples from each other with an optimal margin. This involves orienting the separating hyper-plane to be perpendicular to the shortest line separating the convex hulls of the training data for each class, and locating it midway along this line.

Let the separating hyper-plane be defined by

$x.w + b = 0$ (19)

where w is its normal. For linearly separable N number of data labeled $\{x_i, y_i\}$, $i=1, 2\ldots$ N, the optimum boundary chosen with maximal margin criterion is found by minimizing the objective function

$$E = \frac{1}{2}\|w\|^2 + C \sum_i L(\xi_i)$$

Subject to $(x_i \cdot w + b)y_i \geq 1 - \xi_i$ for all i. (20)

where ξ_i is a "slack" variable that represents the amount by which each point is misclassified, L is a cost function, and C is a hyper-parameter that trades-off the effects of minimizing the empirical risk against maximizing the margin. The solution for the optimum boundary w_0 is a linear

Table 5 Number of training and testing data used

	Normal	Moderate	Severe	M E	Total
Training	42	28	35	21	126
Testing	18	12	15	9	54
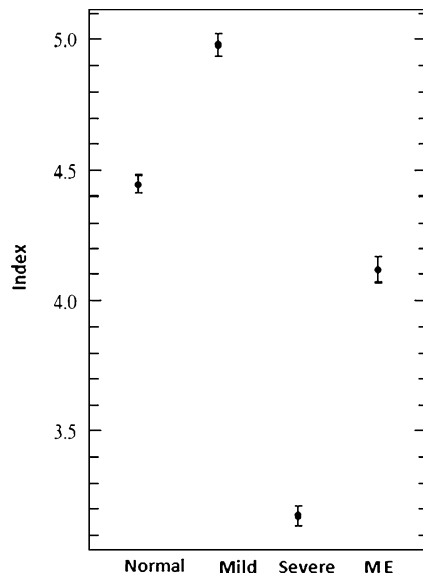
Fig. 5 Box plot of the integrated DR index

combination of a subset of the training data, $s \in \{1 \ldots N\}$ called the *support vectors*. These support vectors define the margin edges.

Most of the real-world data are not linearly separable. In such cases, kernel functions are used. These functions map patterns of pre-processed data into a higher dimensionality space where the data are more separable. In practice, the mapping is achieved by replacing the value of the dot products between two vectors in the input space with the value that results when the same dot product is carried out in the feature space. The dot product in the feature space is expressed by some functions (called the kernels) of two vectors in input space. The polynomial and radial basis function (RBF) kernels are the most commonly used kernels, and they are given by

$$\text{Polynomial kernel} : K\left(x_i, x_j\right) = \left(x_i \cdot x_j + 1\right)^n \tag{21}$$

$$\text{RBF kernel} : K\left(x_i, x_j\right) = \exp\left[-\frac{1}{2}\left(\frac{\|x_i - x_j\|}{\sigma}\right)^2\right] \tag{22}$$

where n is the order of the polynomial and σ is the width of the RBF. Several algorithms extend the basic binary SVM classifier to be a multi-class classifier. Examples consist of one-against-one SVM, one-against-all SVM, half against half SVM and Directed Acyclic Graph SVM (DAGSVM). In this work, we have used one-against-all SVM method.

Results

The range of the extracted five texture features (homogeneity, correlation, short run emphasis, long run emphasis, and run percentage) are shown in Table 4. To test the significance of the features, the ANOVA (Analysis Of
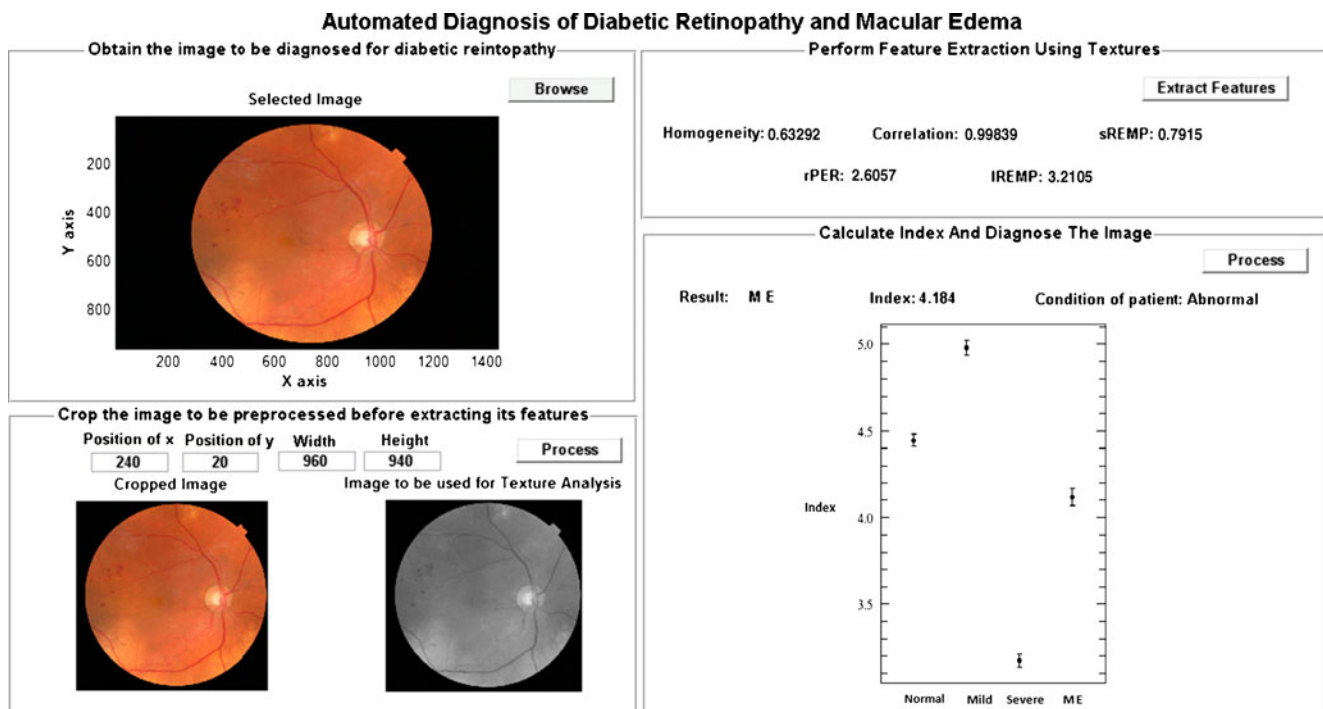
Fig. 6 The snap shot of graphical user interface of our proposed system

Table 6 Accuracy, sensitivity, specificity and positive predictive accuracy (PPA) of the classifier

SVM	TN	FN	TP	FP	Accuracy (%)	+ PV (%)	Sensitivity (%)	Specificity (%)	AUC
Linear Kernel	8	10	31	5	74.1	85.2	75.3	55.8	0.653
Polynomial Kernel with order 1	8	10	31	5	75.3	85.2	76.2	61.1	0.653
Polynomial Kernel with order 2	13	5	35	1	75.3	98.1	88.1	93.9	0.847
Polynomial Kernel with order 3	18	0	34	2	85.2	93.5	98.9	89.5	0.972
RBF Kernel	12	6	36	0	72.2	100	85.7	100	0.833

Variance) test was used. We assumed a null hypothesis that there is no difference among the means of each feature in the various classes. A p-value is a measure of probability that a difference between the means happened by chance. In general, the null hypothesis is rejected if the p-value is less than 0.05 or 0.01, corresponding to a 5% or 1% chance, respectively, of the null hypothesis being true. Accordingly, these fives features can be considered to be clinically significant because their 'p' values are very low (<0.0001). It can be seen from the table that these values are higher for *normal* images than the *diabetic retinopathy* images.

Three-fold stratified cross validation method was used to test the SVM classifier. The whole dataset was split into three parts (roughly) such that each part contains approximately the same proportion of class samples as the original dataset. Two parts of the data (training set) were used for classifier development and the built classifier was evaluated using the remaining one part (testing data) Table 5. This procedure was repeated three times (folds) using a different part for testing in each case. Then the average of all the three results was calculated to get the accuracy, sensitivity, specificity and positive predictive accuracy. Sensitivity is the probability that a test will produce a positive result when used on diseased population. The features were fed to the SVM classifier and the results are tabulated in Table 6. The SVM classifier with a polynomial kernel of order 3 was able to effectively predict correctly about 85.2% of unknown class data with a sensitivity of 98.9%, specificity of 89.5% and positive predictive accuracy of 93.5% (as illustrated in Table 6). The ROC curves obtained using the SVM classifiers with various kernel functions are depicted in Fig. 4, and the corresponding AUC values are presented in Table 6. As indicated, the SVM classifier with the polynomial kernel of order 3 resulted in the highest AUC of 0.972. Thus, the results presented in this work illustrate that it is possible to identify patients with diabetic retinopathy by using the SVM classifier (Table 6).

Integrated diabetes retinopathy index (IDRI)

We also developed an Integrated Diabetic Retinopathy Index (IDRI) which is made up of the following features:

Run percentage, contrast, short run emphasis, and homogeneity. This index, represented by Eq. 23, can be used as an overall indicator for determining the various stages of DR. The IDRI values for the various DR classes are shown in Table 7. The box plots of the IDRI for the various classes (Fig. 5) clearly illustrate the discriminatory capacity of this index for the different classes.

Integrated DRIndex (IDRI)

$$= \frac{RunPer*Contrast*ShortRunEmphasis}{Homogeneity} \quad (23)$$

Figure 6 shows the snap shot of graphical user interface of our proposed system. The image to be analyzed can be selected by pressing the *Browse* button. On clicking the *Process* button (lower left-hand corner) after specifying the cropping size, the selected image will be cropped for further analysis. The *Extract Features* button, when clicked, will use the image processing techniques to extract the five texture features from the selected pre-processed image and to display the same. Finally, the *Process* button at the lower right-hand corner is used to calculate the IDRI for that image and classify it into one of the four DR classes.

Discussion

Computer grading of the severity of three early lesions namely hemorrhages and microaneurysms, hard exudates, and cotton-wool spots, and the classification of non-proliferative diabetic retinopathy (NPDR) based on these three types of lesions was studied [1]. The agreement rates between the computer system and the reading center in determining individual lesions were 82.6%, 82.6%, and 88.3% using the 430 images for hemorrhages and micro-

Table 7 Range of values for integrated DR index (IDRI)

Features	Normal	Moderate	Severe	ME	P value
IDRI	4.4450± 0.170	4.9811± 0.130	3.1758± 0.115	4.1188± 0.112	<0.0001

aneurysms, hard exudates, and cotton-wool spots. Their proposed criteria for computer classification produced results that were comparable with those provided by human experts and thus, the criteria can become a useful clinical aid to physicians for screening, diagnosing, and classifying NPDR.

The presence of microaneurysms is one among the other early signs of diabetic retinopathy. Its diagnosis when the disease is at the early stage can help prevent damages to the diabetic eye. A decision support system (DSS) for the automated screening of early signs of diabetic retinopathy for deducing the presence of microaneurysms was developed and tested [18]. Their results suggested that by biasing the classifier, sensitivity and specificity of 100% and 67% respectively could be achieved.

Four different kinds of retinal conditions, namely, *normal* retina, *moderate NPDR*, *severe NPDR* and *PDR* were automatically classified using area and perimeter of RGB layers and a neural network classifier [14]. They demonstrated an accuracy of more than 80%, a sensitivity of more than 90% and a specificity of 100%. Three classes namely, *normal*, *NPDR* and *PDR* were automatically classified using blood vessels, exudates, and texture parameters and feedforward neural network [11]. Their proposed method was able to identify the unknown class with an accuracy of 93%, sensitivity and specificity of 90% and 100% respectively.

A low cost screening method to identify the normal and abnormal fundus images based on exudates and lesions using statistical classifier and local-window-based verification strategy was proposed [8]. They were able to identify all the retinal images with exudates with 100% accuracy and truly normal images with 70% accuracy. The *normal, mild, moderate, severe* and *prolific DR* classes were automatically classified using higher order spectra features and support vector machine (SVM) classifier [26]. They used 300 fundus images and demonstrated a sensitivity of 82% for the classifier with the specificity of 88%. Five groups: *normal* retina, *mild*, *moderate*, *severe NPDR* and *PDR* were automatically classified using features: blood vessels, exudates, microaneurysms and haemorrhages in a support vector machine classifier [27]. Their proposed method demonstrated a sensitivity of more than 82% and specificity of 86%.

In our current work, significant features namely homogeneity, correlation, short run emphasis, long run emphasis, and run percentage were extracted. We studied SVM classifiers with different kernel functions in order to choose the best classifier for automatic identification. The SVM classifier with polynomial kernel of order 3 is able to accurately identify the unknown class with an accuracy of 85.2%, sensitivity, and specificity of 98.9% and 89.5% respectively. However, the sensitivity of the system can be further improved by using additional more significant texture features. Moreover, the use of a larger number of diverse fundus images for training and testing can increase the robustness of the proposed system.

The novelty of this work is the development of an integrated DR index that has a good discriminatory power among the different DR classes. It can be seen from the Table 7 and Fig. 5 that, one single index value clearly distinguishes different classes with 100% accuracy. It can also be seen from the Table 6 and Table 7 that, IDRI performs better than any of the classifiers in identifying the different classes. IDRI does not require the rigorous training and easy to use. The Index can also be employed to assess the efficacy of diabetic medication and insulin administration.

The programs for the feature extraction using image processing techniques and for the SVM classifier for the automatic identification of the DR classes were written in MATLAB 7.0.4.

Conclusion

Diabetic retinopathy is a progressive eye disease caused due to prolonged diabetes. It can cause loss of vision, if not detected at the early stage. We have proposed an automated technique to identify normal, NPDR, PDR, and ME classes using texture parameters and SVM with polynomial kernel function of order 3. Our computer based system can identify different stages with an average accuracy of 85.2% with sensitivity and specificity of 98.9% and 89.5% respectively.

Finally, we have gone one step further and formulated an Integrated Diabetes Retinopathy Index (IDRI) composed of texture features, given by Eq. 23. This Integrated IDRI can be employed for the diagnosis of normal and different diabetic retinopathy stages, and is found to effectively distinguish all the different classes as shown by Table 7 and Fig. 5. The advantage of this Integrated Index is that, one needs to only look at the value of just one integrated index by looking at how much it deviates from its normal value in order to make the proper diagnosis.

References

1. Samuel, C. L., Elisa, T. L., Yiming, W., Ronald, K., Ronald, M. K., and Ann, W., Computer classification of a non-proliferative diabetic retinopathy. *Arch. Ophthalmol.* 123:759–764, 2005.
2. Fong, D. S., Aiello, L., Gardner, T. W., King, G. L., Blankenship, G., Cavallerano, J. D., Ferris, F. L., and Klein, R., Diabetic retinopathy. *Diab. Care* 26(1):226–229, 2003.
3. Vallabha, D., Dorairaj, R., Namuduri, K. R., and Thompson, H., Automated detection and classification of vascular abnormalities

in diabetic retinopathy, 38th *Asilomar Conference on Signals, Systems and Computers*, 2004.

4. Albregtsen, F., Statistical texture measures computed from gray level run length matrices, 1995.

5. Gardner, G., Keating, D., Williamson, T., and Elliott, A., Automatic detection of diabetic retinopathy using an artificial neural network: A screening tool. *Br. J. Ophthalmol.* 80:940–944, 1996.

6. Ong, G. L., Ripley, L. G., Newsom, R. S., Cooper, M., and Casswell, A. G., Screening for sight-threatening diabetic retinopathy: Comparison of fundus photography with automated color contrast threshold test. *Am. J. Ophthalmol.* 137(3):445–452, 2004.

7. Li, H., Hsu, W., Lee, M. L., and Wong, T. Y., Automated grading of retinal vessel caliber. *IEEE Trans. Biomed. Eng.* 52:1352–1355, 2005.

8. Wang, H., Hsu, W., Goh, K., and Lee, M., An effective approach to detect lesions in colour retinal images. In: *Proceedings of the IEEE Conference on Computer Vision and Pattern Recognition*, pp. 181–187, 2000.

9. Hayashi, J., Kunieda, T., Cole, J., Soga, R., Hatanaka, Y., Lu, M., Hara, T., and Fujita, H., A development of computer-aided diagnosis system using fundus images, Proceeding of the 7*th* *International Conference on Virtual Systems and MultiMedia* (VSMM 2001), pp. 429–438, 2001.

10. Tan, J. H., Ng, E. Y. K., and Acharya, U. R., Study of normal ocular thermogram using textural parameters. *Infrared Phys. Technol.*, 2009.

11. Nayak, J., Bhat, P. S., Acharya, U. R., Lim, C. M., and Kagathi, M., Automated identification of different stages of diabetic retinopathy using digital fundus images. *J. Med. Syst.*, 2008.

12. Weszka, J. S., and Rosenfield, A., An application of texture analysis to material inspection. *Pattern Recognit.* 8:195–200, 1976.

13. Guan, K., Hudson, C., Wong, T., Kisilevsky, M., Nrusimhadevara, R. K., Lam, W. C., Mandelcorn, M., Devenyi, R. G., and Flanagan, J. G., *Diabetes* 55:813–818, 2006.

14. Wong, L. Y., Acharya, U. R., Venkatesh, Y. V., Chee, C., Lim, C. M., and Ng, E. Y. K., Identification of different stages of diabetic retinopathy using retinal optical images. *Inf. Sci.* 178:106–121, 2008.

15. Galloway, M. M., Texture classification using gray level run length. *Comput. Graph. Image Process.* 4:172–179, 1975.

16. Niemeijer, M., van Ginneken, B., Staal, J., Suttorp-Schulten, M., and Abramoff, M., Automatic detection of red lesions in digital color fundus photographs. *IEEE Trans. Med. Imaging* 24(5):584–592, 2005.

17. Tuceryan, M., and Jain, A. K., Texture analysis. In: Chen, C. H., Pau, L. F., and Wang, P. S. P. (Eds.), *Handbook of Pattern Recognition & Computer Vision*, 1993.

18. Kahai, P., Namuduri, K. R., and Thompson, H., A decision support framework for automated screening of diabetic retinopathy. *Int. J. Biomed. Imaging* 1–8, 2006.

19. Bremananth, R., Nithya, B., and Saipriya, R., Wood species recognition system using GLCM and correlation, *Proc. IEEE Computer Society, Int. Conf. ARTCOM* 27–28:615–619, 2009.

20. Gonzalez, R. C., and Woods, R. E., *Digital image processing*, 2nd edition. Prentice Hall, New Jersey, 2001.

21. Frank, R. N., Diabetic retinopathy. *Prog. Retin. Eye Res.* 14 (2):361–392, 1995.

22. Bailey, R. R., *Moments in Image Processing*, 2002.

23. Screening for Diabetic Retinopathy in Europe 15 years after the St. Vincent Declaration, 2005. Available from: http://reseau-ophdiat.aphp.fr/Document/Doc/confliverpool.pdf.

24. Silakari, S., Motwani, M., and Maheshwari, M., Color image clustering using block truncation algorithm. *IJCSI Int. J. Comput. Sci. Issues* 4:31–35, 2009.

25. Standards of medical care for patients with diabetes mellitus. *Diabetes Care* 25:33S–49, 2002.

26. Acharya, U. R., Chua, K. C., Ng, E. Y. K., Wei, W., and Chee, C., Application of higher order spectra for the identification of diabetic retinopathy stages. *J. Med. Syst.* 32(6):481–488, 2008.

27. Acharya, U. R., Lim, C. M., Ng, E. Y. K., Chee, C., and Tamura, T., Computer based detection of diabetic retinopathy stages using digital fundus images. *J. Eng. Med.* 223(H5):545–553, 2009.

28. Press, W. H., Flannery, B. P., Teukolsky, S. A., and Vetterling, W. T., *Numerical recipes in C: the art of scientific computing*. Cambridge University Press, New York, 1990.

29. Xiaohui, Z., and Chutatape, O., Detection and classification of bright lesions in colour fundus Images. *Int. Conf. Image Process.* 1:139–142, 2004.